JOURNAL OF MATERIALS SCIENCE 36 (2001) 2743–2752

Flexural behavior of three-axis woven carbon/carbon composites

WEN-SHYONG KUO*, TSE-HAO KO‡
*Department of *Aeronautical Engineering and ‡Materials Science, Feng Chia University, Taichung, Taiwan, R.O.C*
E-mail: wskuo@fcu.edu.tw

KUO-BING CHENG
Department of Textiles, National Taipei University of Technology Taipei, Taiwan, R.O.C

KUN-YIAN HSIEH
Department of Textile Engineering, Feng Chia University, Taichung, Taiwan, R.O.C

This work examines the processing characteristics and flexural behavior of 3D woven carbon/carbon composites. Two types of the composites have been made, both having 3-axis orthogonal structures. The first combines solid rods along the axial direction. The rod, 1 mm in diameter, is composed of unidirectional carbon fibers and a phenolic resin. The second is a conventional type composed of carbon yarns in all axes. Both preforms were then impregnated by the phenolic resin. Matched molds were used to enhance fiber packing and to cure the resin under a hot press. The green composites were then heat-treated at various temperatures ranging from 200° through 1000° C. The second set of specimens was made by applying multi-cycle impregnation and carbonization. Flexural tests were carried out for these two sets of specimens. Their responses to the load and the induced damage behavior have been examined. The use of rods enhances fiber packing and reduces fiber crimp, leading to higher material performance. Decomposition of the resin due to the heat-treatment results in weak interfacial bonding and compressive failure in axial yarns. The efficiency of densification has been examined. The induced damage configurations vary significantly in these specimens, as a result of the processing. Some unique modes associated with the 3D structure are discussed.

1. Introduction

Carbon/carbon (C/C) composites represent a unique class of materials with many attractive properties. Their high-temperature properties and wear-resistant natures lend themselves to a wide range of applications [1–4]. In applying such materials, however, one concern is the structural integrity. They are considerably weaker than conventional polymer-matrix composites primarily because the pyrolysis introduces voids and cracks in the carbon matrix. Defects of these kinds are often intense in textile, C/C composites [4–6]. Larger voids may appear between bundles because the polymeric precursors—usually phenol-formaldehyde, furane, or thermoplastic pitch—are difficult to impregnate fully. Smaller pores can occur between fibers due to chemical decompositions of the resin that evolves low-molecular compounds such as unreacted phenol, short-chain polymers, and water. During carbonization, the matrix shrinks because of the evolution and condensation of the resin, usually resulting in residual stresses and cracks [7, 8]. Without a sound matrix, fibers are unable to contribute their strength effectively. Densification of the porous matrix is therefore necessary to refill voids and reduce defects. In this regard, access to voids deep in the interior is most important.

Most of the works concerning processing characteristics of C/C composites were based on thin panels made by stacking fabrics [4–8]. Due to the aforementioned defects and inherently weak fiber/matrix bonding, laminated C/C panels are susceptible to interlaminar stresses; separation of plies is a common type of composite failure. Obviously, using three-dimensional (3D) preforms can be a solution [9–13]. Despite their importance and long history of development for defense and aeronautical use, related works aiming at processing-property relationships of 3D C/C composites are very few in the open literature [1, 10–13]. Knowledge learned from 2D panels may not be applied to 3D composites. One apparent difference is that very little dimensional change can occur in multidirectionally reinforced composites because of the fibers. As shrinkage is restricted, residue stresses arise and possibly cause cracks within the matrix. Usually, 3D C/C composites are characterized by higher void content because the fiber architecture is more complex and the composites are thicker. Difficulties often arise

during impregnation of resin into thick 3D preforms. Thus, the efficiency of multi-cycle densification can be notably lower.

This paper examines the fabrication, microstructures and damage behavior of 3D C/C composites. Two types of preforms have been made, including one that incorporates solid carbon/phenolic rods in the axial direction. The notion of using solid rods in 3D C/C composites is not unprecedented in high-tech applications [1, 11]. Yet the related academic research has been absent in the literature. This work makes an effort for a basic understanding toward this class of materials.

2. Material processing

The material processing involves four major steps. The first is fabrication of rods made of carbon fibers and phenolic resin. The second is formation of 3D woven preforms with or without the rods embedded. The third is impregnation and curing of the phenolic resin. The last is the pyrolysis of the resin under various temperatures.

2.1. Carbon/phenolic rods

The use of solid rods was intended to avoid, or at least reduce, fiber crimp—a problem often inevitable in conventional 3D composites because of the flexible nature of fibers. Crimp in fibers can raise many undesirable problems. Even a minimal level of fiber crimp can result in a disproportionate loss of stiffness and strength. To make rods with unidirectional fibers, the technique of pultrusion has been adopted [12]. A large number of the rods composed of carbon fibers and phenolic resin have been produced. The carbon tow (Toho HTA-7) was a PAN-based, high-strength type with a 12k tow size, and the resin was a phenol-formaldehyde type.

The rods are designed to be circular and 1 mm in diameter. In the pultrusion, the die, 0.60 m in length, was set at 60° C at the front, 140° C at the middle, and 160° C at the back. The increasing temperature profile allows a gradual curing of the resin. The drawing speed was set at 300 mm/min. The rods were cut after reaching 2 m long. The fiber volume fraction of the rods was 58.8%. Note that a high fiber packing (>70%) is possible with pultrusion, provided that a suitable tow size is used.

2.2. 3D weaving

To make 3D preforms, the concept of orthogonal weaving was adopted. Two setups for different purposes were assembled. One was designed to combine the rods along the axial direction; the other was a conventional design, using yarns in all axes. Both setups arrange axial (z-axis) bundles in a 5×10 pattern, as illustrated in Fig. 1a. In the setups, shuttles carrying two 12k tows of carbon yarns move in two transverse (x and y) directions. The rod-reinforced preform is labeled YYR, and the all-yarn preform is YYY. In the labels, Y denotes yarn and R denotes rod, and the three symbols represent the bundle types along the x, y, and z directions, respectively. Table I lists the construction of the resulting composites.

The YYR preform was approximately 24×10 mm in the cross-section, and the YYY preform was about 24×8 mm. The YYY was thinner because the axial yarns, unlike the rods, are shapeable when interlaced by the weaving yarns. The weaving process resulted in interlacing loops on the surface and a 3-axis, orthogonal structure in the interior. Fig. 1b shows the representative unit cell of the internal structure for the YYR preform. The cross-sections of the x- and y-axis yarns are closely rectangular, according to the microscopic observations. The unit cell for the YYY preform is similar, except for the cross-sectional shape of the yarns. Note that the unit cell represents the internal structures rather than the entire composite that contains loops on the surface.

TABLE I Construction and fiber volume fractions of the specimens

label	YYR	YYY
x-axis	24k yarn	24k yarn
y-axis	24k yarn	24k yarn
z-axis	12k rod	12k yarn
molding thickness (mm)	7.5	6.5
V_{fx} (%)	21.0	12.2
V_{fy} (%)	21.0	14.5
V_{fz} (%)	10.5	12.2
V_{f} (%)	52.5	38.8

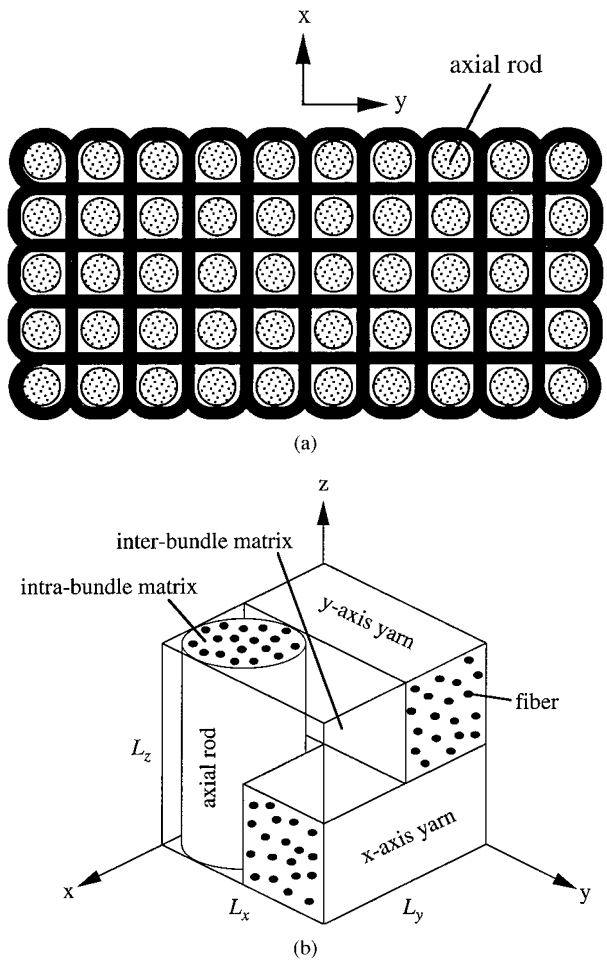

Figure 1 Schematic of the YYR; (a) cross-section showing 5×10 arrangement of axial rods and, (b) unit cell representing internal structure.

2.3. Resin impregnation and curing

For subsequent resin impregnation, the preforms were cut into 120 mm pieces. The preform was impregnated

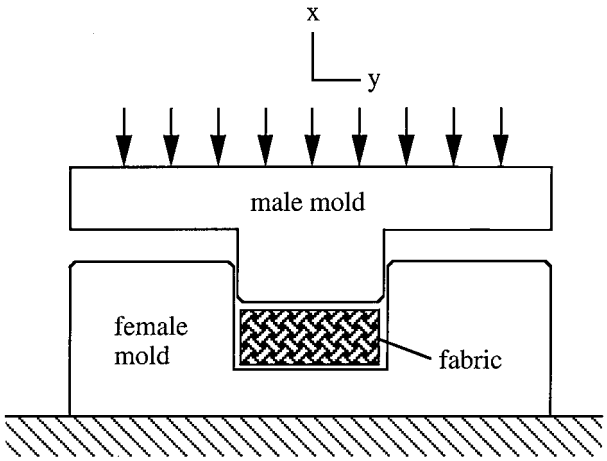

Figure 2 Illustration of the matched mold used in making the green composites.

with the phenolic resin by the method of resin transfer molding (RTM). The RTM mold consists of a cover and an aluminum base with a cavity slightly larger than the preform. The phenolic resin infiltrated into the preform under a vacuum condition. After resin impregnation, the cover was removed, and the base containing the wetted preform was placed within a vacuum oven at 70° C for 6 hours and 80° C for 4 hours, allowing solvents to escape.

To cure the resin, the impregnated preform was heated and pressed under a hot-press. T-shaped male molds were designed to press the impregnated preforms, as shown in Fig. 2. The YYR preform, about 10 mm in thickness, was pressed into 7.5 mm in thickness; the YYY, about 8 mm in thickness, was pressed into 6.5 mm in thickness. Note that the YYR, if pressed into 6.5 mm, can lead to compressive crash in the rods. In conventional processing of 2D C/C panels, applying a rather high pressure is a common practice that enhances fiber packing and reduces void content. In comparison, the 3D preforms were pressed only slightly; the 3D structures can be otherwise harmfully distorted.

With the mold remaining closed, the preform was then cured at 80° C for 1 hour, 130° C for 3 hours, and 160° C for 6 hours; the heating rate between these temperatures was set at 20° C/hour. The cured composite is termed as *green* in this paper.

2.4. Pyrolysis

To study effect of pyrolysis temperature, five sets of the green composites were prepared. Each set consists of three 100 mm-long specimens, which were machined from the 120 mm-long green composites by cutting both ends. Five heat-treatment temperatures were then examined: 200°, 400°, 600°, 800°, and 1000° C. The specimens were heat-treated within a high-temperature oven under a flowing nitrogen atmosphere. The specimens were heated at 0.5° C/min to the designated temperature, followed by cooling to room temperature at approximately 2° C/min. After the heat-treatment, the density was measured.

Three sets of specimens were also made under two, three and four-cycle densification, respectively. Each densification cycle comprised impregnation, curing, and carbonization to 1000° C.

3. Material characterization

3.1. Fiber distribution

Often, fiber content in 1-D and 2D composites can be measured by using a resin-digestion method, which can similarly be applied in the present materials. However, this method measures the overall fiber content rather than distribution of fibers along each axis, which is crucial for 3D composites. For the present composites, fibers are distributed in three axes, and the fiber volume fractions are calculated by using the unit cell.

Because the number of carbon filaments within a yarn is a constant, the fiber volume fraction along the i-axis ($V_{\mathrm{f}i}$) can be expressed as

$$V_{\mathrm{f}i} = \frac{\pi d_{\mathrm{f}}^2 l_i N_i}{4 L_x L_y L_z}, \tag{1}$$

where N_i is the number of filaments within the bundle (Table I), d_{f} is the fiber diameter (7 μm for the carbon fibers), l_i is the length of the i-axis bundle within the unit cell, and L_i is the unit cell dimension of the preform defined in Fig. 1b. The overall fiber content (V_{f}) is thus the sum of V_{fx}, V_{fy}, and V_{fz}.

Equation 1 calculates the fiber content in the preform. When an impregnated preform is compressed, the overall volume decreases while the fiber volume remains unchanged. The fiber volume fraction in the composite is thus proportional to the inverse of the thickness.

3.2. Flexural test

Three-point bending tests were conducted on specimens of length 100 mm, and testing span of 70 mm. Three specimens were prepared in each set of composites. The specimens were placed with the y-axis parallel to the edge of the cross-head. The cross-head speed was set at 2 mm/min. Both the cross-head displacement and the load were measured. The cross-head was halted after apparent damage had appeared in the specimen.

The flexural modulus and flexural strength can be calculated from the slope at the initial linear portion and the ultimate load, respectively, as follows:

$$E = \frac{L^3}{4bh^3}\frac{\Delta P}{\Delta \delta} \tag{2}$$

$$\sigma = \frac{3 P_{\mathrm{u}} L}{2bh^2} \tag{3}$$

where L, b, and h are testing span, specimen width, and thickness, respectively; ΔP and $\Delta \delta$ are increments in load and deflection within the linear portion; P_{u} is the ultimate load. Both equations, originated from the beam theory, are commonly used in characterizing the flexural behavior of materials. Care should be taken in interpreting the flexural strength that calculates the maximum stress within a linearly elastic beam loaded in three-point bending, as the present materials are *not*

linearly elastic at the ultimate load, at which damage has developed. Thus, the equation would better be interpreted as a way of normalizing the ultimate load.

After the test, microscopic observations on the induced damage were conducted. A mounting scheme was adopted to preserve the initially developed damage. Each specimen was immersed into a box containing low-viscosity epoxy resin, which was then cured under vacuum. The mounted specimens were sliced along the desired cross-section, followed by a standard grinding-and-polishing process.

4. Results and discussions

4.1. Bundle geometry

The rods and yarns in the resulting composites differ mainly in cross-sectional shape. Fig. 3 shows typical cross-sections of the YYR and the YYY. The rods in the YYR are straight and arranged in an orderly manner, because the transverse yarns prevent the rods from moving in lateral directions. The *y*-axis yarns, periodically squeezed by the rods, remain straight in their centerlines (Fig. 3a) and become closely rectangular in the cross-sections (Fig. 3b). On the other hand, the YYY

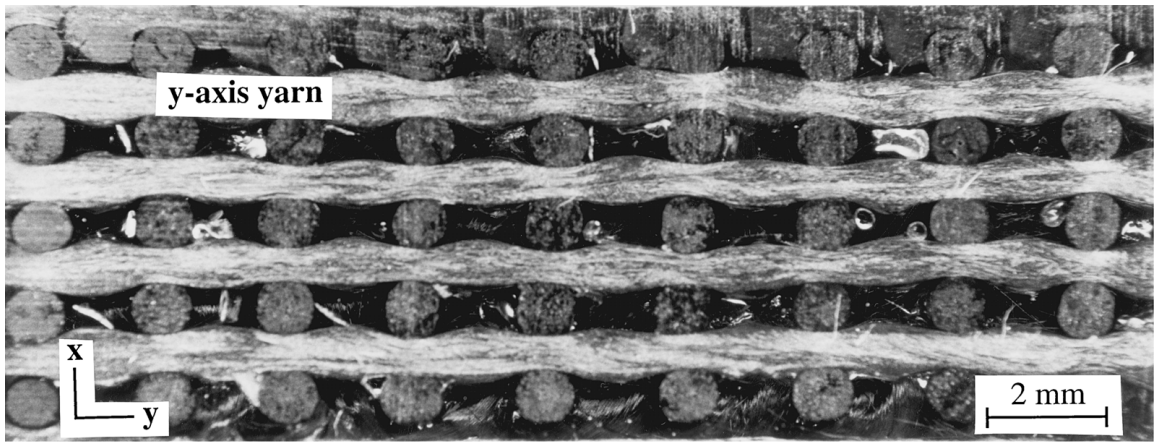

(a) xy-section of the YYR composite

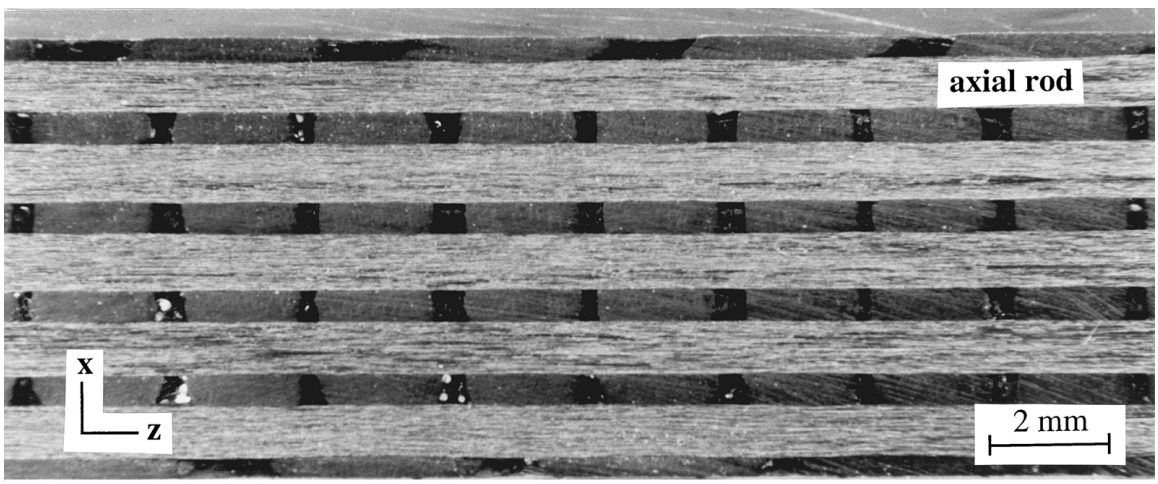

(b) xz-section of the YYR composite

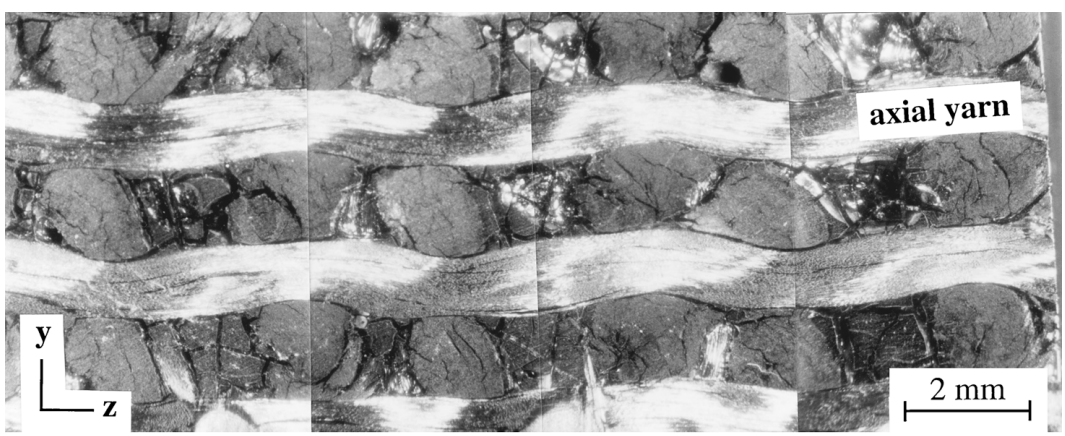

(c) xz-section of the YYY composite

Figure 3 Typical cross-sections showing internal structures of the specimens.

shows periodically undulated axial yarns (Fig. 3c), as a result of the 4-step weaving processes. Yarn undulation is commonly seen in 3D preforms because of the flexible nature of yarns.

Table I lists the calculated fiber volume fractions for the composites. The reduced volume is attributed to expelling of excessive resin and/or elimination of voids. For the YYR, V_{fx} and V_{fy} are nearly identical, while V_{fz} is much lower. For the YYY, the three components are very close. Although both preforms were made under nearly identical conditions, the use of solid rods has resulted in a more compact preform. The V_{fx} and V_{fy} in the YYR are significantly higher than their counterparts in the YYY.

4.2. Flexural behavior

Typical acquired load-deflection curves for the YYR composite under the first-cycle carbonization are shown in Fig. 4a. The curve of the green composite is also shown. During the heat-treatment, the matrix shrinks and pores are created. For the specimen treated at 200° C, the slopes of the initial linear regions were reduced only marginally. When the temperature increased to 400° C, both the slope and the maximum load were considerably decreased. Still, drops in the slope and load were most apparent from 400° to 600° C, suggesting that within this range the chemical reactions are most active. Above 600° C, the materials behaved differently. The initial linear portions of the curves become less apparent, and the nonlinear portions lengthen. No sudden drops occur in these curves, suggesting a pseudo-plastic behavior. The results of the multi-cycle densification are shown in Fig. 4b. With increasing number of cycles, the maximum loads increase regularly. The most notable change is the disappearance of the high-load region. For the four-cycle densified specimen, the curve drops sharply after reaching the peak load, indicating brittle failure. The respective results of the YYY composite are shown in Fig. 5. In general, this YYY composite responds in a similar manner to the change of the heat-treatment temperature and the number of densification cycles.

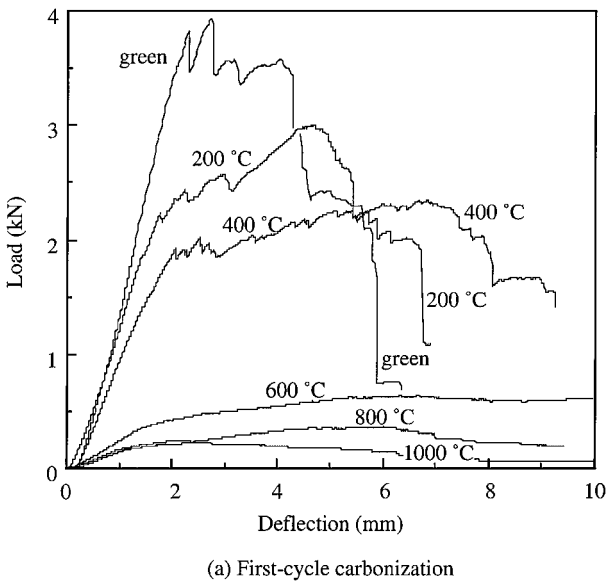

(a) First-cycle carbonization

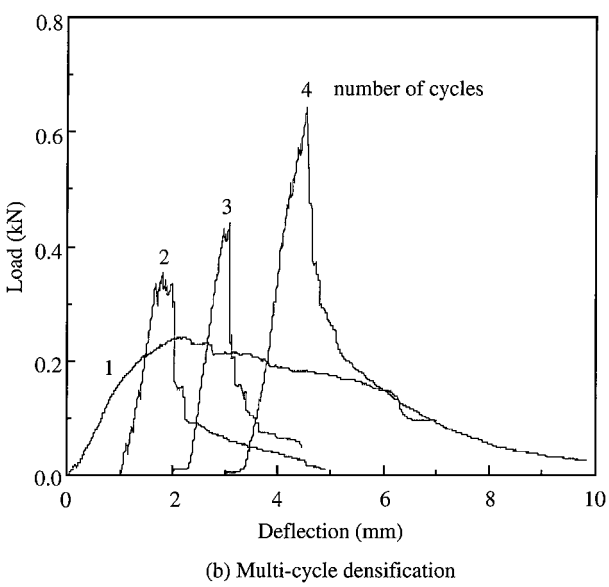

(b) Multi-cycle densification

Figure 4 Loading curves of the YYR composites.

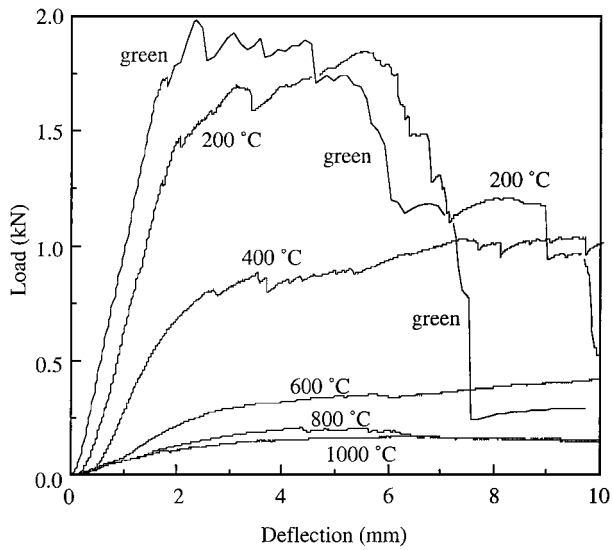

(a) First-cycle carbonization

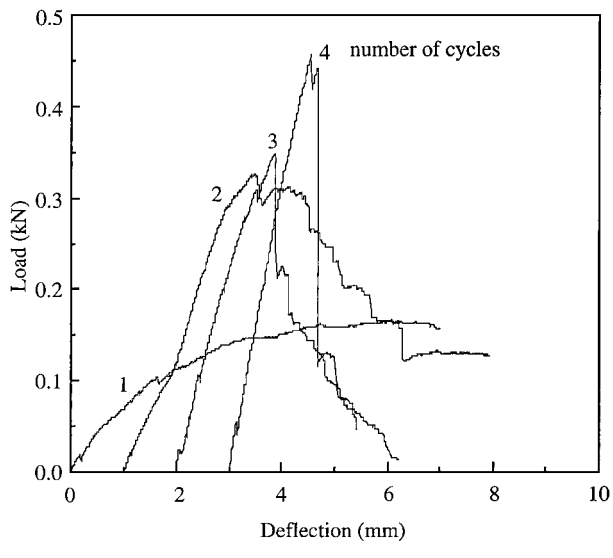

(b) Multi-cycle densification

Figure 5 Loading curves of the YYY composites.

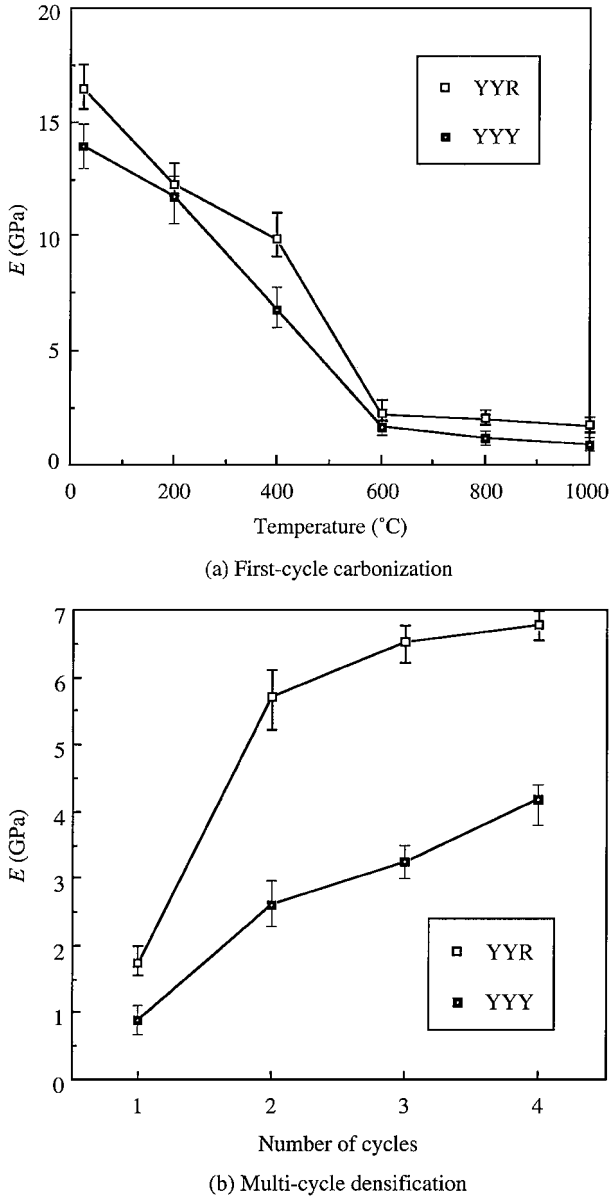

Figure 6 Measured flexural moduli of the specimens.

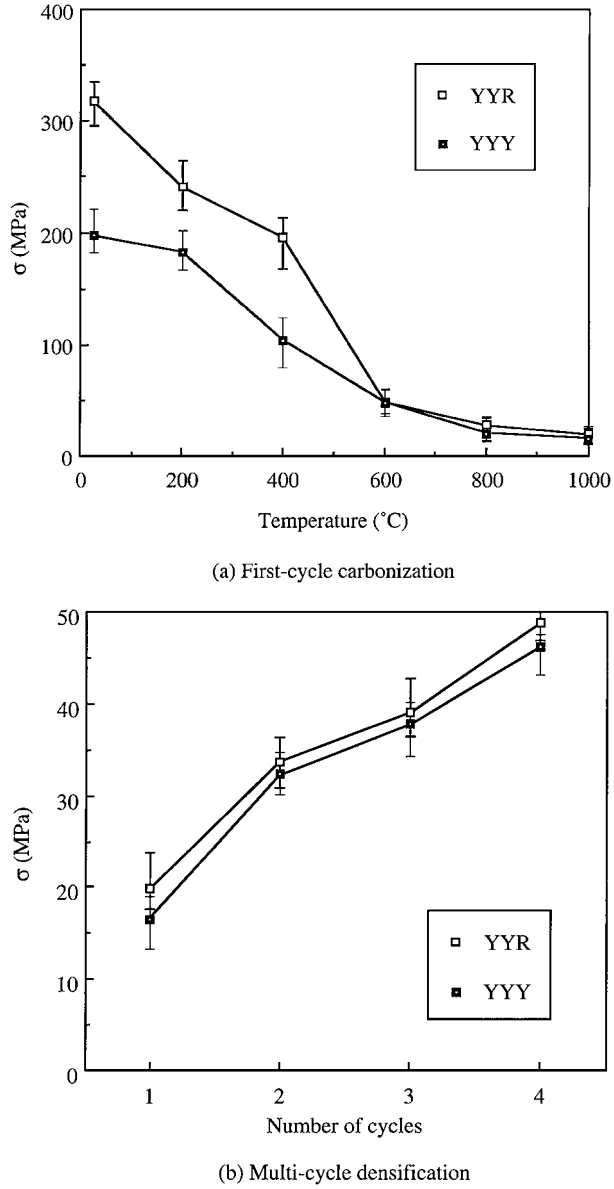

Figure 7 Measured flexural strengths of the specimens.

Fig. 6 shows the results of the measured flexural modulus. The symbol represents the average of three specimens. The green composites, viewed as heat-treated at 25° C, are indeed polymer-matrix composites with relatively sound matrix and strong interface. When the temperature increases, the weakened matrix is unable to hold fibers. The modulus drops significantly up to 600° C and becomes minimal above that. The composites gain modulus most effectively from one to two cycles of densification. The efficiency of refilling the matrix decreases with the number of cycles. The YYY composite, despite possessing no less axial fiber content, is much less stiff than the YYR composite. This discrepancy demonstrates the influence of fiber deformation on the composite modulus.

Results of the calculated flexural strength are shown in Fig. 7. In many ways both the flexural strength and the flexural modulus are similar in responding to change in the processing temperature and the number of densification cycles. Nevertheless a difference is that below 400° C the YYY composite is considerably weaker than the YYR. Beyond 600° C, however, the weaving-caused undulation appears to be less influential, since yarn buckling can lead to greater deformation. As a result, both the YYY and the YYR composites become equally weak. The strength is regained remarkably with the densification cycle. The efficiencies of strengthening are about the same for both the YYR and the YYY composites.

4.3. Density

Fig. 8 shows the measured composite densities. In the first-cycle carbonization, the loss of weight is mainly attributed to decomposition of the matrix; fibers under the processing conditions are essentially unaffected. The YYR composite is denser than the YYY counterpart, simply because the YYR contains more fibers, which are heavier than the phenolic resin. The densities increase with the densification cycle, but the values are still much lower than for 2D C/C panels under the same number of densification cycles [9]. Three reasons may account for this. First, the present 3D composites are lower in fiber content, thus bringing down the density.

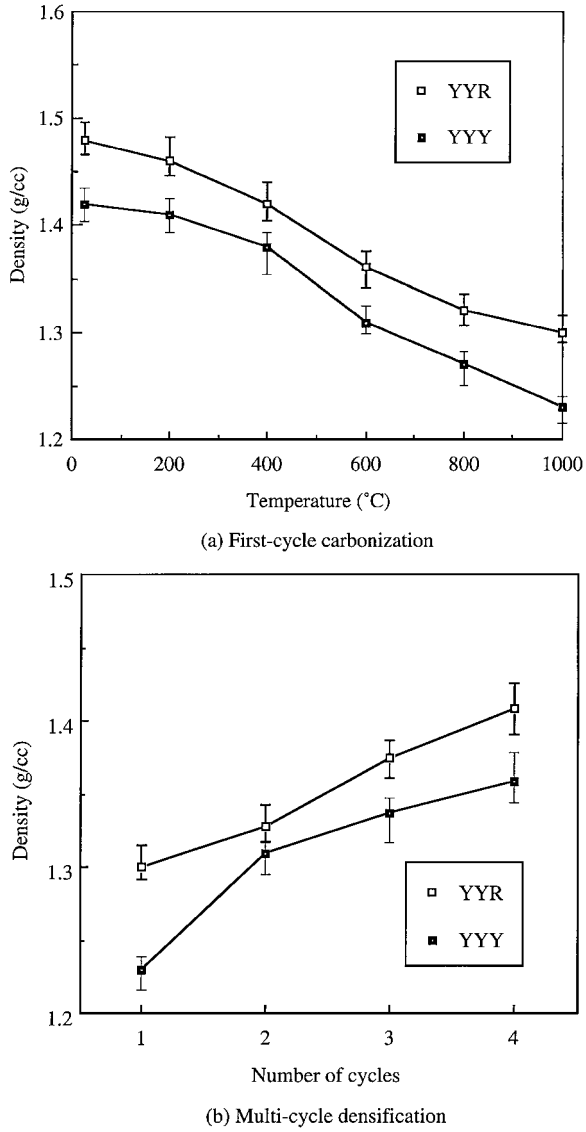

Figure 8 Measured densities of the specimens.

Second, the present composites are thicker and are more complex in yarn structures than conventional 2D C/C panels. As a result, a complete resin impregnation is more difficult. Third, during resin curing, the present composites were compressed into a fixed thickness, unlike 2D panels that are hot-pressed under a high pressure, which can effectively eliminate voids and make the composites denser.

4.4. Damage behavior

Fig. 9 shows the YYR specimens of the first-cycle heat-treatment. Crack openings can be seen on the green composites. Fig. 10 is a xz-section of a green YYR specimen. Tensile rupture of the axial rods was the major mode that led to material failure and sudden decreases in the loading curves. Compressive failure in the form of kink bands was occasionally observed at the rod at the top layer, where the compressive stress is the highest. As the temperature rises, crack openings become invisible, although specimens treated at 200° and 400° C are still damaged primarily in tensile fracture; weaving loops on the surface cover up the damaged rods.

For specimens treated at higher temperatures, the damage shifts to the compressive side. The matrix decomposes almost entirely at 1000° C, weakening fiber bonding and causing voids in inter-yarn and intra-yarn spaces—both leading to buckling of compressed yarns. A typical micrograph of the rod after the first-cycle carbonization is shown in Fig. 11, revealing a large number of voids inside the rods. The damage configurations of the YYY specimens are similar.

Compressive failure, generally a minor mode in the present composites, becomes dominant only for those with weak matrix—namely, those first carbonized at higher temperatures. Yet the configurations of this

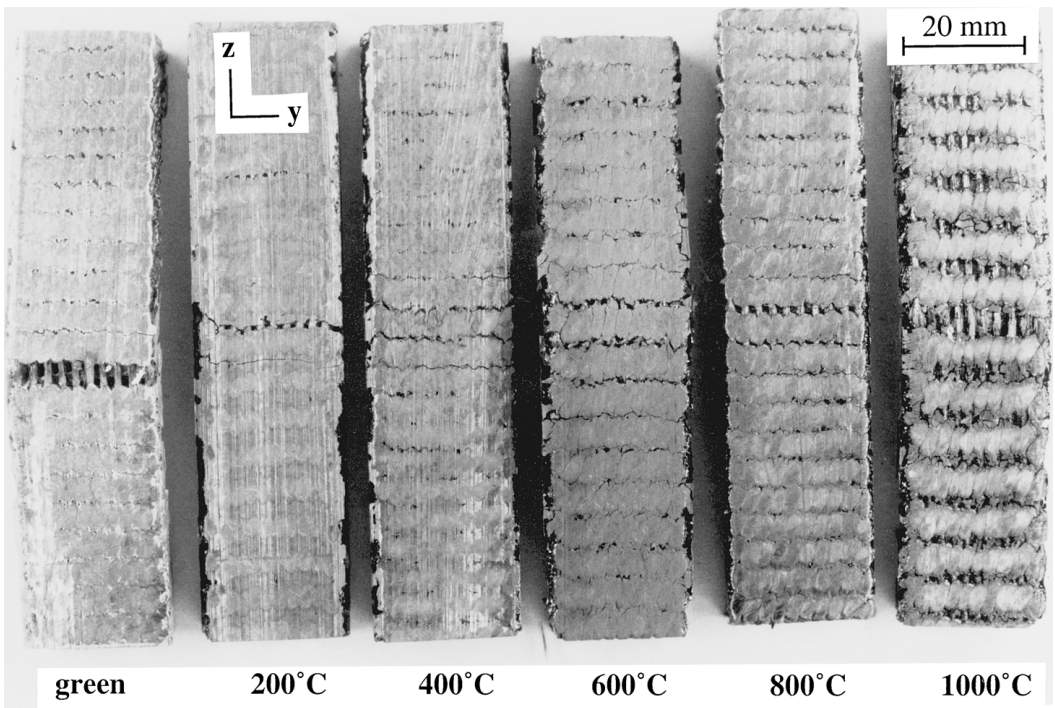

(a) tensile side

Figure 9 The first-cycle treated YYR specimens, showing influence of the processing temperature. (*Continued*.)

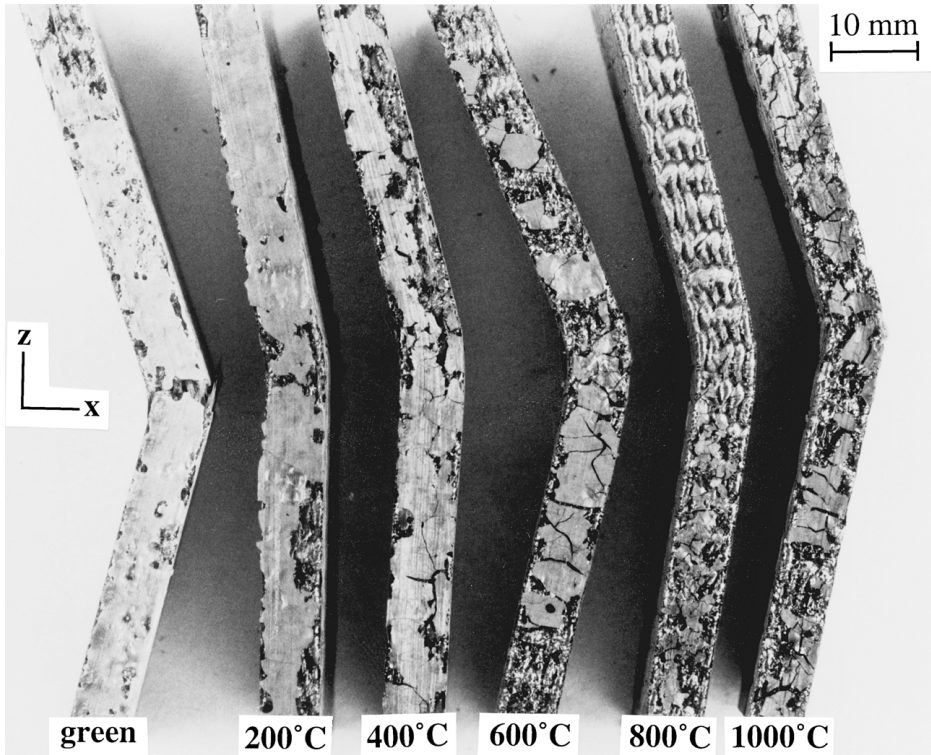

(b) side view

Figure 9 (*Continued*.)

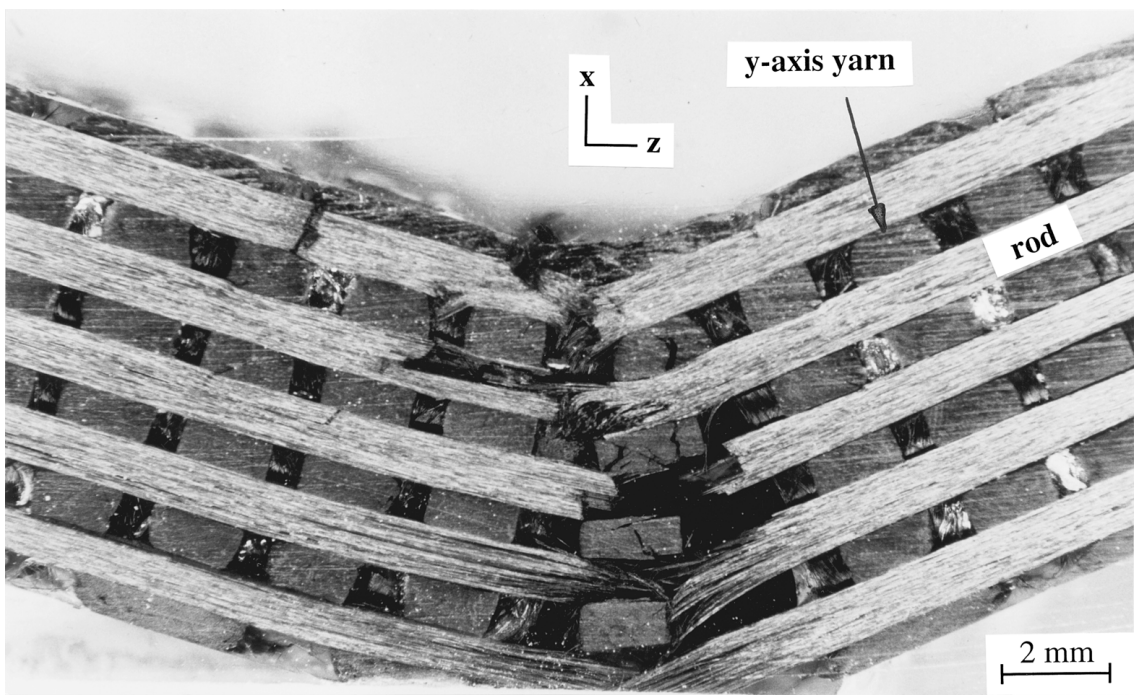

Figure 10 A green YYR specimen damaged due to tensile fracture in the rods.

failure mode are intriguing, as a result of the 3D network of fibers and different matrix behavior. Fig. 12 compares different modes of compression-induced damage. Fig. 12a is a fractured green YYR specimen showing fiber microbuckling that forms kink bands within the rod. The growth of the kink bands must be affected by the 3D structure. First, kink bands are more likely to occur near inter-bundle regions, which are weaker than bundles. Second, the growth of fiber buckling can bounce back after hitting the boundary of the bundle, forming V-shaped kink bands. The presence of kink bands reveals satisfactory matrix and interface strengths; otherwise the mode shown in Fig. 12b is more likely to occur.

When treated at higher temperatures, the axial bundles can fail in a different way. Fig. 12b shows a buckled rod in the YYR composite carbonized at 1000° C. Instead of forming kink bands, the fibers undergo

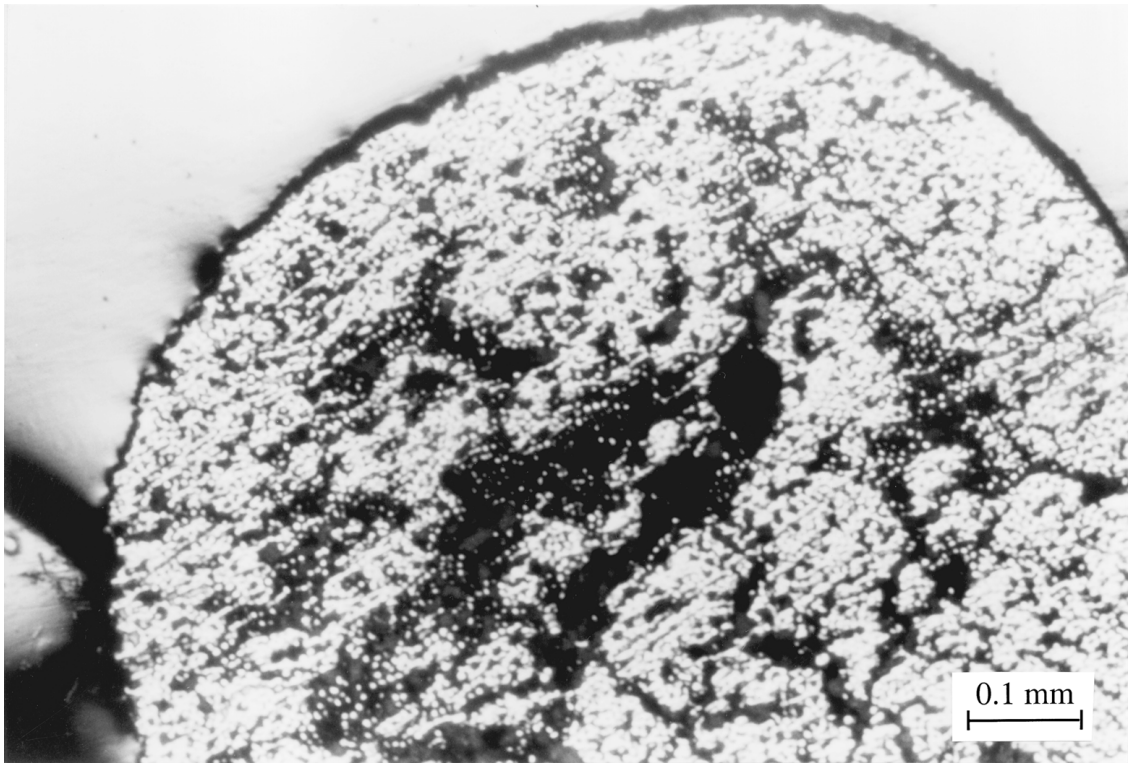

Figure 11 A rod in a YYR specimen after the first-cycle carbonization at 1000° C, leaving intra-bundle voids (dark areas).

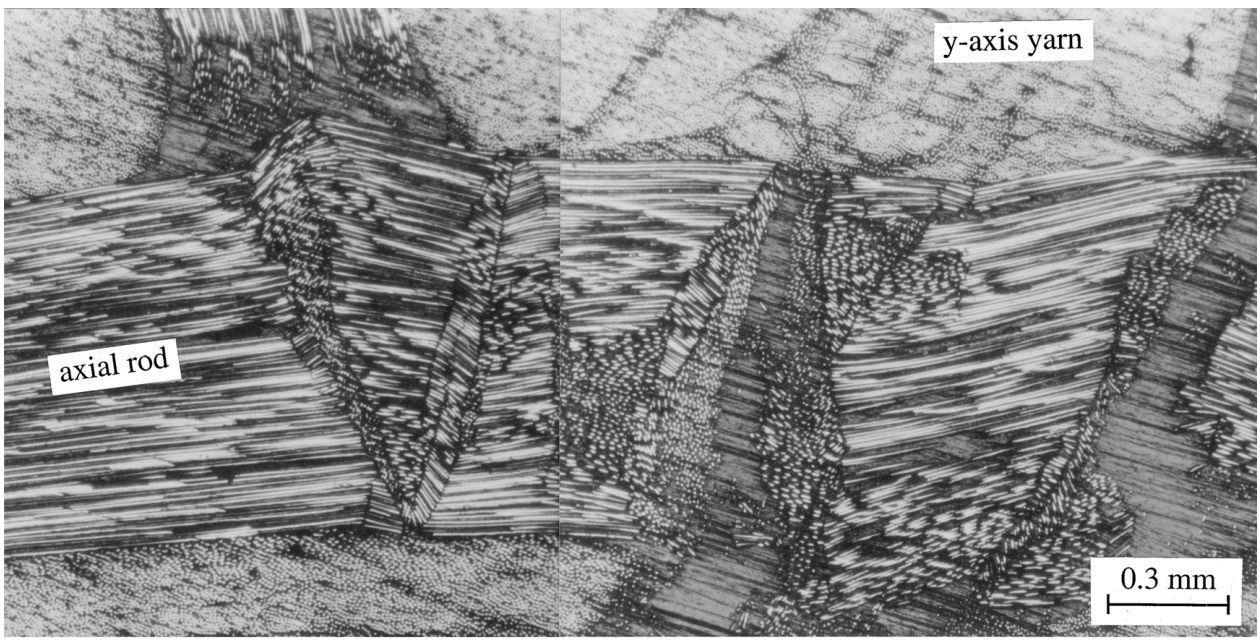

(a) the green YYR composite

Figure 12 Failure modes in the compressive side of a YYR composite: (a) V-shaped kink-bands and (b) splitting-and-bulging in the axial rods. (*Continued*.)

splitting-and-bulging. Splitting is indeed fiber/matrix debonding, while bulging is a form of fiber buckling. Apparently, splitting can occur only when fiber bonding is weak, and bulging can occur only when there is an empty space adjacent to the bundle. This mode reveals the importance of fiber bonding and matrix integrity. Thus, enhancing the interfacial strength and eliminating voids in inter-bundle regions must be helpful in resisting splitting-and-bulging.

Tensile failure is the dominant mode for most of the specimens. When multiple densification is applied, voids in inter-bundle regions can be refilled. Once the compressive strength is enhanced, failure tends to shift to the tensile side, and thus the overall capability in resisting the flexural load is also enhanced. The density is still low, and the results indicate that there is room for making denser composites. The key lies not in more cycles of processing, but in the efficiency of densification. In other words, refilling voids deep inside, especially in intra-bundle regions, is the most critical challenge in the fabrication of thick, 3D C/C composites.

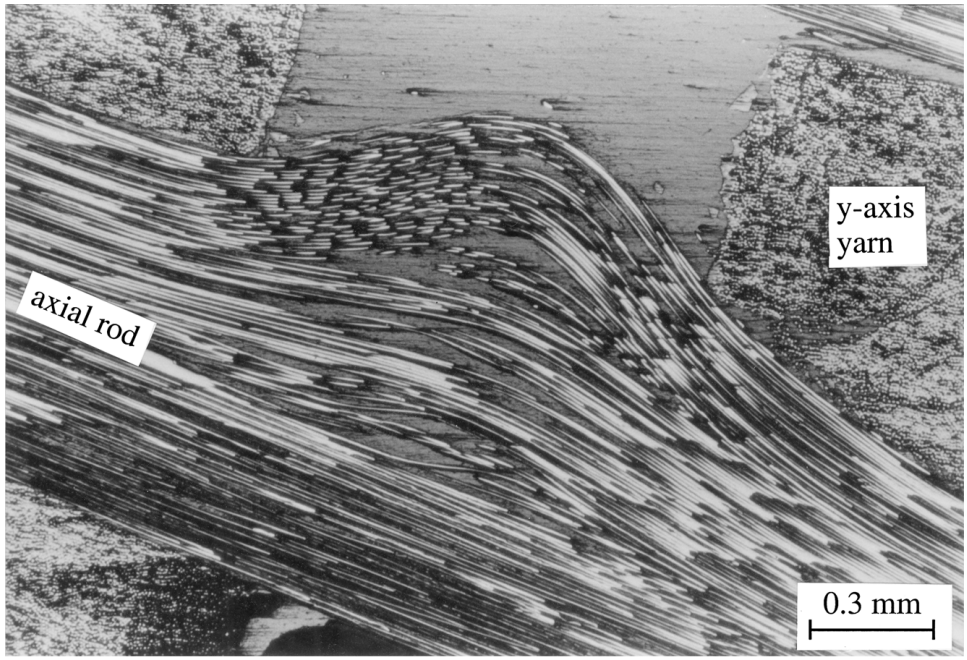

(b) the YYR composite treated at 1000˚C

Figure 12 (*Continued.*)

5. Conclusions

During the first-cycle carbonization, the responses of the materials can be divided into three stages. Up to 400° C, the loss of flexural modulus and strength is marginal. The specimens are linearly elastic to some extent. Tensile fracture in axial bundles dominates the material failure. From 400° to 600° C, the chemical reactions are most active, leading to significant decreases in the density, flexural modulus, and flexure strength. From 600 to 1000° C, the flexural modulus stays at the same level and flexural strength decreases only slightly. The linear region becomes less apparent, and no sudden fall can be seen in the loading curves. Compressive failure becomes dominant. The materials can be largely deflected without apparent fractures, suggesting a pseudo-plastic behavior. The differences between the YYR and the YYY composites in the flexural properties also diminish.

In the multi-cycle densification, the matrix refilling is more effective in early cycles; the density, flexural modulus and strength increase considerably. Although there are still significant pores inside the materials, the refilling efficiency is reduced during the third and the fourth cycles. Impregnating voids inside the thick composites is the key to improving the materials. After four cycles of densification, the composites become more brittle, and the failure mode shifts to the tensile side.

Because of the network of 3D fibers, two modes of compressive failure have been observed. The V-shaped kink bands was the major mode in the green composites. When the temperature increases, the axial bundles tend to fail in splitting-and-bulging. Matrix integrity and interfacial strength are the keys to determine these modes. Using rods has been proved to be beneficial in enhancing fiber packing and reducing fiber crimp, both resulting in improved mechanical behavior.

Acknowledgments

The authors wish to thank the Feng Chia University (FCU-RD-87-01) and the National Science Council of Taiwan, R.O.C. (NSC 88-2216-E-035-002) for the support of this research.

References

1. E. FRIZER, *Carbon* **25** (1987) 163.
2. J. D. BUCKLEY, *Ceramic Bulletin* **67** (1988) 364.
3. G. SAVAGE, in "Carbon-Carbon Composites" (London: Chapman & Hall, 1993) p. 323.
4. T. H. KO and W. S. KUO, *Polymer Composites* **19** (1998) 618.
5. F. GAO, J. W. PATRICK and A. WALKER, *Carbon* **31** (1993) 103.
6. K. ANAND and V. GUPTA, *ibid.* **33** (1995) 739.
7. J. JORTNER, *ibid.* **30** (1992) 153.
8. H. WEISSHAUS, S. KENIG and A. SIEGMANN, *ibid.* **29** (1991) 1203.
9. G. RELLICK, *ibid.* **29** (1990) 589.
10. P. B. POLLOCK, B. J. HINDS, R. J. TEDERS and C. G. KOCHER, *ibid.* **31** (1993) 992.
11. C. R. THOMAS, "Essentials of Carbon–Carbon Composites" (Cambridge: The Royal Society of Chemistry, 1993) p. 119.
12. J. L. PERRY and D. F. ADAMS, *Carbon* **14** (1976) 61.
13. W. S. KUO, T. H. KO and Y. C. CHI, *Polymer Composites* **20** (1999) 460.

Received 21 April
and accepted 13 December 2000